# A Novel Structural Analysis for a Cylinder-Forming Block Copolymer Thin Film Using Neutron Reflectivity Aided by Transmission Electron Microtomography

**Ken-ichi Niihara,[†] Ukyo Matsuwaki,[†] Naoya Torikai,[‡] Hironori Atarashi,[§] Keiji Tanaka,[§] and Hiroshi Jinnai*[,†]**

*Graduate School of Science and Engineering, Kyoto Institute of Technology, Matsugasaki, Kyoto 606-8585, Japan, Neutron Science Laboratory, High Energy Accelerator Research Organization, 1-1 Oho, Tsukuba, Ibaraki 305-0801, Japan, and Department of Applied Chemistry, Faculty of Engineering, Kyushu University, 744 Motooka, Nishi-Ku, Fukuoka 819-0395, Japan*

*Received June 16, 2007; Revised Manuscript Received July 17, 2007*

ABSTRACT: Microphase-separated structures of a poly(deuterated styrene-*block*-2-vinylpyridine) (dPS-*b*-P2VP) block copolymer in thin films were studied by neutron reflectivity (NR) and transmission electron microtomography (TEMT). The dPS-*b*-P2VP block copolymer shows a cylindrical morphology in the bulk state. The block copolymer was spun-coated on a Si substrate, which was extensively annealed (170 °C for 14 days) before the NR experiments. The annealed thin film showed a featureless NR profile, the reflectivity monotonically decreased with the increasing scattering vector along the depth direction of the thin film, $q_z$. The portion of the dPS-*b*-P2VP block copolymer thin film used in the NR experiment was examined by TEMT, from which a three-dimensional (3D) morphology of the block copolymer thin film was successfully obtained. The 3D image clearly showed that the microphase-separated structure inside the thin film had a cylindrical morphology with some order along the depth, but almost no in-plane order. In order to analyze the NR profile by a conventional model fitting method, a model structure that exhibits a concentration profile is necessary as an initial "guess". In this study, two different models, i.e., (i) hexagonally packed P2VP cylinders laying parallel to the Si substrate based on the known lattice parameters, and (ii) experimentally obtained TEMT 3D structure, were proposed. The concentration profiles evaluated from these two models were used as the initial guesses in the fitting of the calculated profiles to the experimentally obtained NR profile, $R_{\text{exp}}$. It was found that the fitting based on the former model failed, while the fitting based on the latter one had an excellent fit to the $R_{\text{exp}}$. This result demonstrates that the microphase-separated structures that are NOT perfectly periodic nor oriented can still be analyzed by our new technique.

## 1. Introduction

Block copolymers exhibit highly periodic and various types of microphase-separated structures due to the immiscibility between the dissimilar (A and B) sequences.[1] Classical block copolymer nanostructures include spheres of A(B) on a body-centered cubic lattice in a B(A) matrix, cylinders of A(B) on a hexagonal lattice in a B(A) matrix, and co-alternating lamellae. Several complex (bicontinuous) nanostructures—the perforated lamellar (PL), gyroid (G) and double-diamond (D) morphologies—may develop if the copolymer composition falls within a narrow range between the cylindrical and lamellar morphologies. When the microphase-separated structures are confined in a thin film whose thickness is on the order of 10 to 100 nm, the surface interaction (between the block copolymer and substrate or between the block copolymer and air surface) as well as the confinement significantly affects the microphase-separated structures.[2] The block copolymer thin films have drawn considerable attention in many technological areas such as microelectronics[3−6] and nanoporous films.[7,8] For example, Guarini et al. reported that block copolymer thin films can be used as the mask layers for dense nanoscale dot patterning.[3] They also presented the following possible applications of the nanometer-scale structures: the high surface area substrates for capacitors and biochips, quantum dot arrays for nonvolatile memories, silicon pillar arrays for vertical transistors or field-emission displays, etc.

In order to understand the self-assembling morphologies of the block copolymer thin films, it is particularly important to study in detail the self-assembling processes and the resulting morphologies. Neutron (or X-ray) reflectivity (NR) is one of the most useful methods to investigate microphase-separated structures of block copolymer thin films.[9] It provides a concentration (density) profile of one of the components with the very high precision of 0.5 nm. A significant amount of structural information about block copolymer thin films, e.g., the location of junctions between the dissimilar sequences and chain ends inside the microdomains and the interfacial thickness, have been obtained.[10−13]

Although powerful, NR with a conventional model fitting method first requires a hypothesized concentration profile for data analysis. The initial concentration profile is assumed using some stacked layers perpendicular to the film surface so that it can simulate the microphase-separated structure in the block copolymer thin film. The concentration profile assumed along the *Z*-direction, i.e., the direction normal to the substrate, is subsequently used to fit the experimentally obtained NR profile.[14] This "fitting" protocol of the concentration profile to the NR profile heavily depends on the initial concentration profile.[15] Thus, up until recently, NR has been used for rather simple morphologies that can be easily hypothesized, e.g., a lamellar morphology parallel to the substrate.[10−13] Although

---

[*] To whom correspondence should be addressed: e-mail: hjinnai@kit.ac.jp.
[†] Graduate School of Science and Engineering, Kyoto Institute of Technology.
[‡] Neutron Science Laboratory, High Energy Accelerator Research Organization.
[§] Department of Applied Chemistry, Faculty of Engineering, Kyushu University.

10.1021/ma071334c CCC: $37.00

some of the above applications seek to take advantage of the cylindrical microdomains in the block copolymer thin film, there are only a few studies dealing with cylinders,[16,17] and to the best of our knowledge, there are no studies dealing with other types of microphase-separated structures in the block copolymer thin films due to some difficulties in assuming the appropriate initial concentration profiles for these morphologies. Therefore, it is critical to establish a methodology to estimate the initial concentration profiles.

Dynamic secondary ion mass spectroscopy (DSIMS) is one of the candidates to *directly* measure the concentration profile of a specific elements along the *Z*-direction.[17−19] The disadvantage of DSIMS over NR is its inferior resolution. Ge et al. examined the surface-induced ordering of the poly(deuterated ethyl acrylate-*graft*-styrene) graft copolymer (dPEA-*g*-PS) thin film by NR and DSIMS.[17] They employed DSIMS to measure the concentration profile of dPEA that was used as the initial model in the fitting protocol. The concentration profile of dPEA after the fitting showed several peaks, the distance of which was taken as the periodicity or interlayer distance of the internal morphologies. However, the concentration profile merely shows the statistically averaged fluctuation of the dPEA concentration, which does not necessarily correspond to the periodicity. Namely, even though the dPEA concentration was directly measured by DSIMS, the type of microphase-separated structures, e.g., lamellae or cylinders, and their arrangements in the thin films still have to be assumed. Since the microphase-separated structures in the thin films are *not* necessarily the same as those in the bulk state,[18,20,21] it is preferable to *directly* observe the microphase-separated structures in the thin film by real-space methods, i.e., microscopy.

Transmission electron microtomography (TEMT) is one of the most powerful microscopic techniques for obtaining real-space three-dimensional (3D) images of the microphase-separated structures.[22−24] A considerable number of studies on the microphase-separated structures of block copolymers have already been reported using TEMT: The chain conformation inside in microdomains,[25] morphologies,[26−29] grain boundary morphologies,[30,31] stability,[32] and self-assembling processes[33−35] of block copolymers were discussed. Although TEMT provides 3D images of nanometer-scale structures, the spatial resolution and measurement volume are still inferior to and smaller than those obtainable by NR. The highest resolution reported to date by TEMT is 0.5−1.0 nm.[24,36] Thus, in order to study local morphologies, e.g., interfacial thickness of the block copolymers, NR is essential.

All three methods mentioned above have advantages and disadvantages based on their nature. The best way to fully characterize the microphase-separated structures of the block copolymer thin films is to combine them. In the present study, we used TEMT for the 3D real-space structures of the block copolymer thin films in order not only to obtain intuitive pictures of the system, but also to evaluate their concentration profile. NR was also employed to obtain statistically averaged global and local structural information based on the TEMT results with even a better spatial resolution (than TEMT).

## 2. Experimental Section

**A. Materials.** The poly(deuterated styrene-*block*-2-vinylpyridine)(dPS-*b*-P2VP) block copolymer was purchased from Polymer Source, Inc., Canada. The number-average molecular weight, $M_n$, of the dPS and P2VP blocks were 102 000 and 38100, respectively. The polydispersity index, $M_w/M_n$, is 1.10. The volume fraction of dPS is 0.73. The scattering length density ($b/v$) of the dPS and P2VP blocks were $6.47 \times 10^{-4}$ nm$^{-2}$ and $1.95 \times 10^{-4}$ nm$^{-2}$, respectively. Here $b$ and $v$ are the scattering length and the molar volume, respectively.

**B. Specimens.** In order to observe the morphology in the bulk state of the dPS-*b*-P2VP block copolymer, a film specimen was prepared by casting a 5 wt % 1,4-dioxane solution for ca. 1 week. The cast film was annealed at 170 °C for 1 day under vacuum. The annealed film was then ultramicrotomed using a diamond knife at room temperature with a Lica Ultracut UCT. The ultrathin section was transferred onto a Cu mesh grid with a polyvinylformal substrate. Prior to the transmission electron microscope (TEM) observations, the ultrathin section was stained by $I_2$ vapor for 3 h.

The block copolymer thin film was prepared by spin-coating from a 4 wt % 1,4-dioxane solution onto the silicon (Si) substrate at 1700 rpm. The thin film was annealed at 170 °C for 14 days under vacuum. The annealed thin film, cut into 7 cm × 4 cm sections from the spun-coated wafer, was first used for the NR experiments, a portion of which was subsequently used for the TEMT experiments.

**C. Neutron Reflectivity.** The NR measurement was carried out using the PORE pulsed-neutron reflectometer[37] at the Neutron Science Laboratory, High Energy Accelerator Research Organization in Tsukuba. In this study, we observed the specular reflection using white neutrons with the wavelength, $\lambda$, ranging from 0.3 to 1.6 nm. The incident angle, $\theta$, was fixed at 0.4, 1.0, and 2.0°, and the angular resolution, $\Delta\theta/\theta$, was kept at 5% by adjusting the width of the two incident slits. An algorithm of Parratt based on a recursive calculation method[14,15] was used to calculate the reflectivity profiles from the scattering length density ($b/v$) profile along the direction perpendicular to the film surface, i.e., along the *Z*-direction. $\chi^2$ of the fitting error between the measured and calculated reflectivities was calculated by

$$\chi^2 = \frac{1}{1 - N} \sum_{i=1}^{N} \left( \frac{R_{m,i} - R_{c,i}}{R_{m,i}} \right)^2 \qquad (1)$$

where $R_{m,i}$ and $R_{c,i}$ are the measured and calculated reflectivities at a specific scattering vector, respectively. $N$ is the total number of measured points. In that fitting protocol, $\chi^2$ were calculated to be as small as possible. A software available on the web, Parratt32,[50] was used in the fitting protocol.

**D. Transmission Electron Microscopy and Transmission Electron Microtomography.** The portion of the dPS-*b*-P2VP thin films used for the NR experiments was made into a TEM section in the following way. First, the thin film was stained by $I_2$ vapor for 3 h and subsequently coated with carbon in order to reduce the charging and to enhance heat transfer during the ultrathin sectioning using the focused-ion-beam (FIB) method (JEM-9310FIB, JEOL Co., Ltd., Japan).[38] We note here that the sectioning without peeling off the block copolymer thin film from the Si substrate became possible using FIB. The section was placed on the Cu mesh grid for the TEM and TEMT experiments. Prior to the TEMT observations, gold particles (diameter: 10 nm) were placed on the ultrathin sections using a gold colloidal solution (GCN005, BBInternational Ltd., U.K.).

The TEM and TEMT observations were carried out using a JEM-2200FS (JEOL Co., Ltd., Japan) operated at 200 kV and equipped with a slow-scan CCD camera (Gatan USC1000, Gatan Inc.) as the detector.[24,28,30,31,33,39,40] Only the transmitted and elastically scattered electrons (electron energy loss of 0 ± 15 eV) were selected by the energy filter installed in the JEM-2200FS (Omega filter, JEOL Co., Ltd., Japan). A series of TEM projections was acquired at tilt angles ranging from −50° to +50° in 1° increments. The tilt series were then aligned by the fiducial marker method[41] using the Au particles and then reconstructed on the basis of the filtered back projection method.[42] Note that the mean alignment error,[43] averaged over all of the fiducial markers used in the alignment, was 0.185 nm, which was less than the pixel resolution regardless of the tilt angles.[39] All alignment and reconstruction procedures were carried out using software developed in our laboratory.

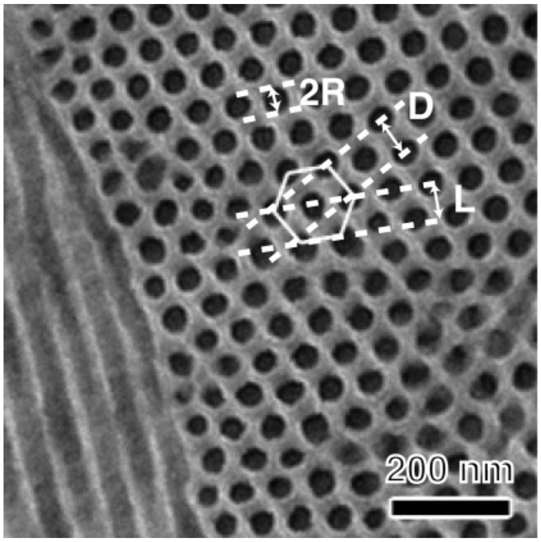

**Figure 1.** TEM micrograph of the dPS-*b*-P2VP in the bulk state. Dark and bright phases correspond to P2VP and dPS microdomains, respectively. The white hexagon indicates the hexagonally packed P2VP cylinders. *R* is the radius of the cylinder. *D* and *L* are the domain spacing and layer distance of the hexagonal packed cylinder lattice, respectively.

**E. Dynamic Secondary Ion Mass Spectroscopy.** The PS (ca. 180 nm thick) was coated on the top of the specimen used in the NR experiments by a floating technique. This coating was necessary because the ion beam is often unstable right after the sample is irradiated by the beam. With the sacrifice of the PS layer, the ion beam becomes stable by the time the ion beam finishes sputtering this PS layer. Thus, when the ion beam starts sputtering the dPS-*b*-P2VP thin film, the beam intensity should become stable so that a quantitative result can be expected. Furthermore, on the top of the PS protection layer, Au (ca. 20 nm thick) was coated in order to avoid any charging of the specimen by the ion beam. The DSIMS measurement was carried out using a SIMS-4000 (Atomika Analysetechnik GmbH). The incident oxygen ion beam was focused onto a 400 $\mu$m × 400 $\mu$m area of the specimen's surface at 4 keV and 45 nA. The incident beam angle was 45°.

## 3. Results and Discussion

**A. Structural Observation in the Bulk State.** Figure 1 shows a TEM micrograph of the dPS-*b*-P2VP in the bulk state. This copolymer self-assembled a typical hexagonal packed cylindrical morphology. The dark circles on the right-hand side of Figure 1 correspond to the edge-on view of the cylindrical microdomains, while the stripe pattern on the left-hand side is a side view of the cylinders. The radius, *R*, of the cylindrical domains was evaluated to be 22 nm. The domain spacing, *D*, and layer distance, *L*, are 68 and 58 nm, respectively. When the cylinder-forming block copolymers were made into thin films, the cylindrical microdomains aligned parallel to the substrate surface due to the strong affinity of one of the block chains to the surface.[40,44]

**B. Neutron Reflectivity Measurement.** The measured NR profile from the dPS-*b*-P2VP, $R_{\mathrm{exp}}$, is shown by the open circles in Figure 2 where the reflectivity, *R*, is plotted vs the magnitude of the scattering vector along the *Z* -direction, $q_z$ ($q_z \equiv (4\pi/\lambda) \sin\theta$). A featureless NR profile was obtained from the thin film, indicating that the microphase-separated structure inside the thin film was not very ordered.

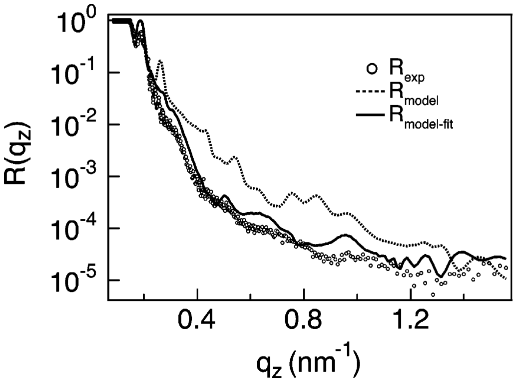

**Figure 2.** NR profile of the dPS-*b*-P2VP thin film (open circles). The dashed line is the calculated reflectivity profile based on the hypothetical model in which the hexagonally packed cylinders are aligned parallel to the substrate. The corresponding $b/v$ is shown by the dashed line in Figure 3b. The dashed line was used as an "initial guess" in the fitting protocol.[14,15] The solid line represents the best-fit NR profile after the fitting [the corresponding $b/v$ is the solid line in Figure 3b] $\chi^2$ of the best-fit NR profile (solid line) was $4.6 \times 10^{-2}$, which was calculated using eq 1.

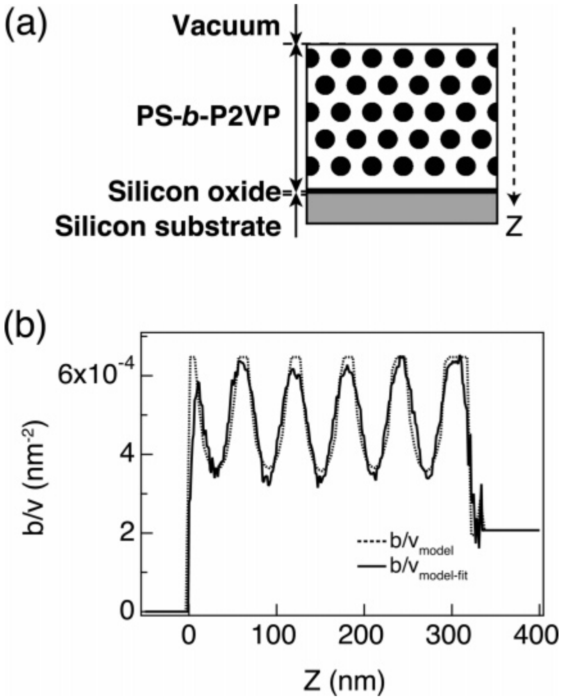

**Figure 3.** (a) Cross-sectional view of hypothesized initial model of dPS-*b*-P2VP thin film cast on Si substrate. Dark circles and white domain are the edge-on view of the P2VP cylinder and dPS matrix, respectively. The *Z*-direction in normal to the film surface. (b) Scattering length density profile, $b/v$, of the dPS-*b*-P2VP. The dashed line is the calculated profile from the hypothesized model shown in part a. The solid line is the calculated $b/v$ profile from the best-fitted reflectivity profile (solid line in Figure 2).

Although $R_{\mathrm{exp}}$ indicated that the microphase-separated structure was rather disordered, let us first assume that the microphase-separated structure formed hexagonally packed cylindrical microdomains in the thin film as illustrated in Figure 3a. The cylinders are assumed to be aligned parallel to the substrate according to the results from previous studies.[16,40,44] The hypothetical model is based on the structural parameters determined from the bulk state, i.e., in Figure 1 and from the film thickness separately measured by atomic force microscopy (AFM). The scattering length density profile along the direction perpendicular to the film surface, i.e., along the *Z*-direction, was calculated from the model, $b/v_{\mathrm{model}}$, which is shown by the dashed line in Figure 3b. Since the $b/v$ is smaller for P2VP than for dPS, the peak-top and peak-bottom in the $b/v$ correspond to the dPS and P2VP phases, respectively. There are five bottoms in Figure 3b, each of which correspond to each layer of the P2VP cylinders. The NR profile based on the model,

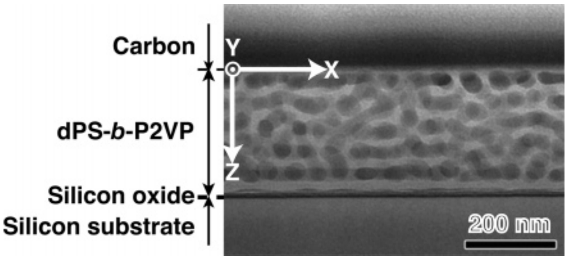

**Figure 4.** Cross-sectional TEM micrograph of the dPS-*b*-P2VP thin film. This micrograph consists of three part, the carbon layer, the dPS-*b*-P2VP thin film and the silicon substrate from the top to bottom of the micrograph. Dark phase and bright phase in the dPS-*b*-P2VP thin film correspond to the $I_2$-stained P2VP and dPS microdomains, respectively. The *X*-, *Y*-directions and *Z*-direction are parallel and perpendicular to the film surface. In the TEMT experiment, the tilt axis was set to be parallel to the *X*-direction.

$R_{\mathrm{model}}$, is also plotted by the dashed line in Figure 2. It is obvious that the $R_{\mathrm{model}}$ did not reproduce the NR profile over the entire range of $q_z$. Subsequently, the algorithm of Parratt based on a recursive calculation method[14,15] was employed to fit the $R_{\mathrm{model}}$ to $R_{\mathrm{exp}}$. The resulting best-fit profile and the corresponding $b/v$ are shown by the solid line in Figure 2 and Figure 3b, respectively. Although the NR profile after the fitting approached $R_{\mathrm{exp}}$, there was still a considerable deviation especially for the large $q_z$. This result again indicates that the microphase-separated morphology was not a simple one as hypothesized. Since the NR profile did not show distinctive peaks, it is intrinsically difficult to have a precise and unique best-fit profile unless we have a realistic model for $b/v$ as the initial guess. Therefore, we employed TEMT to *directly* visualize the 3D morphology of the dPS-*b*-P2VP thin film, which will be used as the initial guess as shown in the following section.

**C. A New Method: Combination of NR and TEMT.** Figure 4 shows a cross-sectional TEM micrograph of the dPS-*b*-P2VP thin film. Note that the cross-sectional section (specimen) for the TEM (and later for the TEMT) experiment was prepared by the FIB method from exactly the same spun-cast sample used in the NR experiments. On the top of the dPS-*b*-P2VP thin film, a carbon layer was coated for protection before the FIB sectioning. Beneath the carbon layer, the dPS-*b*-P2VP thin film morphology can be seen, in which the dark and bright microdomains correspond, respectively, to the P2VP and dPS phases. Underneath the dPS-*b*-P2VP thin film, there was a thin layer of the Si native oxide layer, although it was difficult to see in Figure 4. Note that the Si native oxide layer was confirmed under TEM at a higher magnification (not shown here). The microphase-separated morphology observed under TEM appeared to be a cylindrical domain. The majority of the P2VP cylinders seemed to align parallel to the Si substrate, while some cylinders may be vertically aligned. Compared with the hypothetic model shown in Figure 3a, nevertheless, the cylindrical microdomains turned out to be rather disordered despite of the extensive annealing. Such disordered microdomains, in turn, should definitely produce the featureless NR profile observed in Figure 2.

Since the thickness of the cross-sectional sample was ca. 200 nm, the microphase-separated structure significantly overlapped, and hence the details of the structure were lost along the optical axis of the TEM (*Y*-direction). If the microphase-separated structure had a lamellar morphology parallel to the substrate, the cross-sectional TEM micrograph would more clearly appear, because there would be no overlap. In such a case, the TEM cross-sectional view alone would give a relatively quantitative concentration profile of one of the blocks, from which $b/v$ can be evaluated.

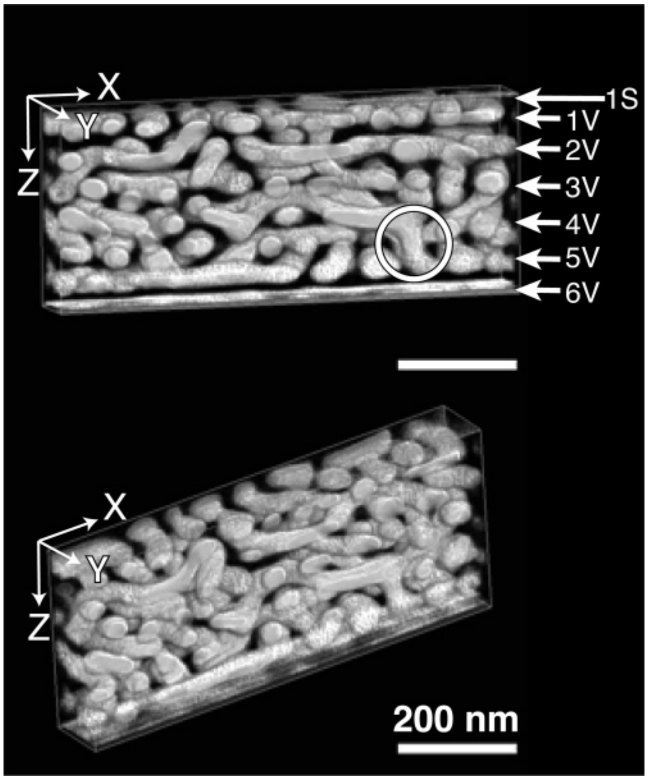

**Figure 5.** Volume rendered 3D images of the dPS-*b*-P2VP thin film from two different view points, in which the dPS microdomain was made transparent. The box size of each 3D image is 720 × 90 × 344 nm. Arrows on the right of the 3D image indicate the P2VP layers.

The cross-sectional sample was tilted in the TEM to take a series of projections. The tilt axis was parallel to the *X*-direction. The reconstructed 3D images of the dPS-*b*-P2VP thin film are displayed in Figure 5 from two different view points, in which only the P2VP phase is shown (the dPS phase is transparent). In Figure 5, the *Z*-direction corresponds to the depth direction of the dPS-*b*-P2VP thin film. The details of the 3D morphology of the dPS-*b*-P2VP thin film were visible in the figure. The volume fraction of the P2VP phase evaluated from the 3D image was 0.28, which was in excellent agreement with the known composition of the copolymer, i.e., 0.27. The average film thickness measured from the 3D image was 344 nm, which was also in good agreement with the AFM result. Note that the 3D image shown in Figure 5 was cropped along the *Y*-direction for viewing clarity (the total thickness in the *Y*-direction was 200 nm). Although the majority of the cylindrical microdomains were oriented parallel to the substrate and formed six layers as indicated by arrows in Figure 5, they did not formed hexagonally packed cylinders as hypothesized in Figure 3a. The same conclusion was drawn for the TEM micrograph [see Figure 4], however, the 3D images strengthened this point even further. In addition, the cylindrical microdomains aligning normal to the film surface that connected the adjacent layers were also displayed by the white circle in Figure 5. It seemed that the cylindrical microdomains were interconnected through such vertical cylinders. It is also confirmed that the P2VP and dPS microdomains wetted the Si substrate and free surface, respectively, demonstrating that the dPS-*b*-P2VP thin film was the asymmetrical-wetting case. The P2VP wetting layer is the bottom layer in Figure 5.

It is very likely that our annealing time may not be sufficient to bring the system to an equilibrium state. We note here that the previous study using dPS-*b*-P2VP with similar molecular weight indicates that the cylindrical morphology was not completely hexagonally packed after annealing the thin film at 180 °C for 2 weeks.[18] On the other hand, Noro et al. claimed that their lamellar-forming dPS-*b*-P2VP with (again) similar molecular weight attained equilibrium by even shorter annealing time (170 °C for 1 week) than ours.[13] Therefore, the annealing time required for bringing the system to its equilibrium state may be morphology-dependent. Closer look at the 3D structure in Figure 5 suggests that the parallel ordering of cylinders near the air and silicon oxide surfaces seems to be better than that of cylinders located at inner film. Since it is well-known that the formation of microdomains in a block copolymer thin film develops first from the surface (air or substrate), this would be another indication that the inner morphology would not represent the equilibrium morphology. In any case, even though the cylindrical morphology in the thin film is not an equilibrium one, it would still be worthwhile to develop a method to characterize the morphology.

The concentration of dPS block was estimated from the 3D image in the following way. First, the 3D image was binarized so that the dPS and P2VP domains become 0 (black) and 255 (white), respectively (we assume 8-bit depth gray scale in this explanation). The voxel intensities of the dPS and P2VP microdomains in the binarized 3D image were then converted to the scattering length densities of the corresponding components. The voxels in the 3D image now have two intensities with a physical meaning. The underlying assumption here is that the two microdomains consist of pure blocks, i.e., either dPS or P2VP. The $b/v$ at a given $Z$ coordinate were first averaged in the $X$-$Y$ plane to estimate the representative $b/v$ at the depth. The obtained $b/v$ at various $Z$s were then stacked to obtain the scattering density profile along the $Z$-direction, $b/v_{\mathrm{TEMT}}$, and shown by the dashed line in Figure 6a. The NR profile based on this $b/v_{\mathrm{TEMT}}$ was obtained from the TEMT experiments, $R_{\mathrm{TEMT}}$, and shown in Figure 6b. Comparing the previous results in Figures 2 and 3, i.e., $R_{\mathrm{model}}$ and $b/v_{\mathrm{model}}$, (i) $R_{\mathrm{TEMT}}$ exhibited a more accurate NR profile than did $R_{\mathrm{model}}$, and (ii) $b/v_{\mathrm{TEMT}}$ had six peaks (as $b/v_{\mathrm{model}}$ did), but their heights were distinctively different from the $b/v_{\mathrm{model}}$, especially in the middle of the thin film (100 nm ≤ $Z$ ≤ 250 nm). The $R_{\mathrm{TEMT}}$ reproduced the $R_{\mathrm{exp}}$ very well at a low $q_z$ ($q_z < 0.4$ nm$^{-1}$), but not in the high $q_z$ region, indicating that the $b/v_{\mathrm{TEMT}}$ (and thus TEMT) captures the global feature of the dPS-*b*-P2VP thin film morphology, but the structural details were lost. In other words, TEMT already offers statistically averaged structural information by itself, but has inferior spatial resolution compared to NR.

The $b/v_{\mathrm{TEMT}}$ was subsequently used as the initial guess for the fitting. The resulting scattering density profile, $b/v_{\mathrm{TEMT-fit}}$, and the corresponding reflectivity profile, $R_{\mathrm{TEMT-fit}}$, after the fitting[14] are denoted by the solid lines in Figures 6a and 6b, respectively. The $R_{\mathrm{TEMT-fit}}$ showed on excellent agreement with the $R_{\mathrm{exp}}$, much better than the $R_{\mathrm{model}}$ shown in the previous section.

The novel methodology proposed in the present study can be extended to the structural studies of the block copolymer thin film with more complicated and disordered morphologies, e.g., the gyroid, perforated layer, etc. We note that the reflectivity alone had difficulty in dealing with these morphologies. In addition, the methodology may also be extended to the off-specular scattering data[15,45-48] as well as specular scattering data, i.e., the reflectivity, because the 3D volume data obtainable from TEMT provide not only the depth, but also in-plane structural information.

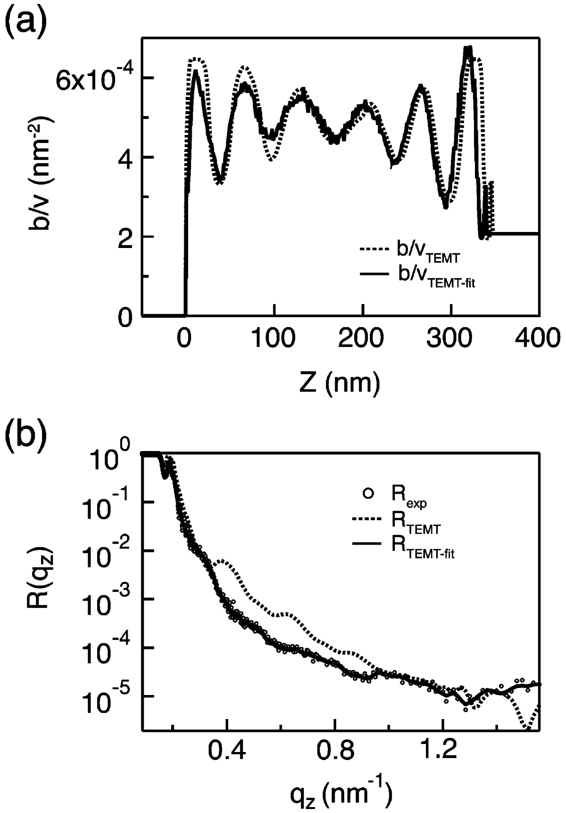

**Figure 6.** (a) Scattering length density profile ($b/v$) of the dPS-*b*-P2VP. The dashed line is the calculated $b/v$ profile from the 3D image obtained by TEMT. The solid line shown in part (b) is the calculated $b/v$ profile from the best-fit reflectivity profile. (b) Reflectivity profile of the dPS-*b*-P2VP thin film. Open circles are the measured NR profile. The dashed line and the solid line represent the calculated reflectivity profile from initial model obtained by TEMT and the best-fit reflectivity profile, respectively. $\chi^2$ calculated from eq 1 was $1.91 \times 10^{-2}$.

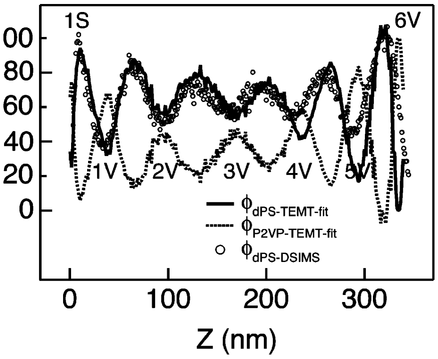

**Figure 7.** Concentration profiles of the dPS-*b*-P2VP thin film, $\phi$. The solid and dashed lines correspond to the concentration of dPS and P2VP, respectively. Letters on the peaks of $\phi$ are used to specify the layers of dPS or P2VP where S and V denote dPS and P2VP, respectively. Open circles are the measured concentration profile of dPS by DSIMS.

**D. Confirmation of the Concentration Profile with DSIMS.** The volume fraction of the dPS and P2VP blocks normal to the substrate ($\phi_{\mathrm{dPS-TEMT-fit}}$ and $\phi_{\mathrm{P2VP-TEMT-fit}}$) are shown, respectively, by the solid and dashed lines in Figure 7. They were calculated from the scattering density profile obtain from the fitting, $b/v_{\mathrm{TEMT-fit}}$, in Figure 6. On the free surface ($Z = 0$ nm, denoted as 1S), $\phi_{\mathrm{dPS}}$ was nealy 100%, demonstrating that the dPS wetted the free surface. In contrast, $\phi_{\mathrm{P2VP-TEMT-fit}}$ was almost 100% at $Z \sim 340$ nm (6V), therefore, the P2VP blocks wetted the substrate surface. This result is consistent with the known fact that the more polar P2VP block (than dPS) wets the polar Si oxide surface.[18,49]

The first peak of $\phi_{\mathrm{P2VP-TEMT-fit}}$ from the free surface (1V) was 66%, which was close to the $\phi_{\mathrm{P2VP}}$ of the {1 0} plane in the bulk cylindrical microdomains, e.g., the layer indicated by the dashed white line in Figure 1. This experimental finding indicates that most of the P2VP microdomains at this depth are cylinders, more or less parallel to the free surface. On the contrary, the peaks deeper inside the thin film, i.e., 2V ~ 4V, had a lower $\phi_{\mathrm{P2VP-TEMT-fit}}$ than that of 1V, indicating that the P2VP microdomains were not completely oriented to the substrate and were connected with the neighbor P2VP layers as seen from the 3D image [see Figure 5]. The deepest P2VP peak from the free surface (5V) had a slightly higher $\phi_{\mathrm{P2VP-TEMT-fit}}$ than that of the first peak (1V) and considerably higher than $\phi_{\mathrm{P2VP-TEMT-fit}}$ of the intermediate peaks. According to the 3D image, the morphology at this depth had characteristics similar to the first peak, i.e., well oriented cylinders. There was observed a sharp depletion zone right above the P2VP wetting layer, which may cause the 5V peak to be sharper and higher.

A secondary ion intensity profile of the negative deuterium ($D^-$) ion was obtained by DSIMS, from which the concentration profile of dPS, $\phi_{\mathrm{dPS-DSIMS}}$, was estimated *independently* from the TEMT and NR(the open circles in Figure 7 together with $\phi_{\mathrm{dPS-TEMT-fit}}$). Although the spatial resolution of DSIMS was not as good as that of either the TEMT or NR, $\phi_{\mathrm{dPS-DSIMS}}$ showed an excellent agreement with $\phi_{\mathrm{dPS-TEMT-fit}}$ , clearly demonstrating that the new methodology combining TEMT and NR provides not only a high-resolution (through NR), but also an intuitive (through TEMT) way of characterizing the block copolymer morphologies.

## 4. Summary

A three-dimensional (3D) microphase-separated structure of a cylinder-forming poly(deuterated styrene-*block*-2-vinylpyridine)(dPS-*b*-P2VP) under confinement was studied by neutron reflectivity (NR) and transmission electron microtomography (TEMT). A featureless NR profile was obtained from the dPS-*b*-P2VP thin film. A model, assuming the hexagonally packed cylindrical microdomains aligning parallel to the substrate, was used to estimate the scattering length density profile, $b/v_{\mathrm{model}}$, along the depth, i.e., the *Z*-direction of the block copolymer in the thin film. A significant discrepancy between the calculated NR profile based on the $b/v_{\mathrm{model}}$, $R_{\mathrm{model}}$, and experimentally obtained NR, $R_{\mathrm{exp}}$, was found over the entire range of the scattering vector, $q_z$. Using $R_{\mathrm{model}}$ as the initial structure, the fitting of $R_{\mathrm{model}}$ to the $R_{\mathrm{exp}}$ by iteratively changing $b/v_{\mathrm{model}}$ was unsuccessful.

In order to obtain a more realistic scattering density profile of the block copolymer thin film, TEMT was employed to image the 3D structure inside the film. The 3D image showed that the structure had a six-layer cylindrical morphology in which the cylindrical microdomains aligned mostly parallel to the substrate, but their in-plane orientation was rather disordered. The scattering density profile was evaluated from the 3D image, $b/v_{\mathrm{TEMT}}$, which was then used to calculate the NR profile, $R_{\mathrm{TEMT}}$. It was found that $R_{\mathrm{TEMT}}$ reproduced the $R_{\mathrm{exp}}$ better than did the $R_{\mathrm{model}}$, especially in the low $q_z$ region. In the high $q_z$, however, a significant deviation between the $R_{\mathrm{exp}}$ and $R_{\mathrm{TEMT}}$ was found. These results indicated that the overall shape of $b/v_{\mathrm{TEMT}}$ reflected the microphase-separated structure but the detailed structural information, such as an interface, was lost. With $R_{\mathrm{TEMT}}$ as the initial structure, the fitting of the NR profile to $R_{\mathrm{exp}}$ has been carried out. The best-fit profile, $R_{\mathrm{TEMT-fit}}$, showed an excellent agreement with the $R_{\mathrm{exp}}$. The scattering length density profile corresponding to $R_{\mathrm{TEMT-fit}}$, $b/v_{\mathrm{TEMT-fit}}$, exhibited six peaks, from the shape of which the middle three layers were found to be the cylindrical microdomains mostly aligned parallel to the substrate, but with a certain amount of vertical alignment. This finding was confirmed by the TEMT 3D image and was distinctively different from the above hexagonally packed cylinder model. The concentration profile of dPS was then calculated from the $b/v_{\mathrm{TEMT-fit}}$, which was *quantitatively* confirmed by dynamic secondary ion mass spectroscopy.

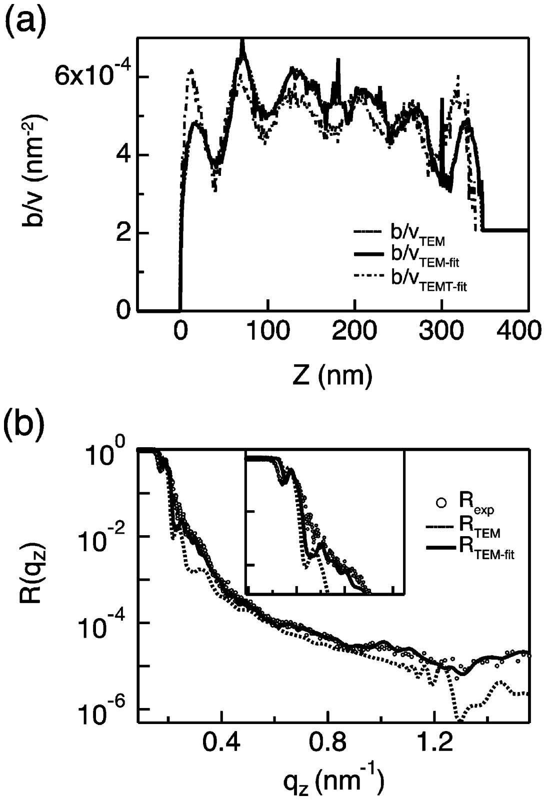

**Figure 8.** (a) Scattering length density profile, $b/v$, of the dPS-*b*-P2VP. The dashed line is the calculated $b/v$ profile from the concentration profile obtained from the cross-sectional TEM micrograph. The solid line is the calculated $b/v$ profile from the best-fit reflectivity profile, which is shown by the solid line in part b. The dashed-dotted line is the $b/v$ obtained from the best-fit using TEMT (that is, the reproduction of $b/v_{\mathrm{TEMT-fit}}$ in Figure 6a). (b) NR profile of the dPS-*b*-P2VP thin film. The open circles are data points measured by NR. The dashed and solid lines correspond to the calculated reflectivity profile from the initial model obtained from the cross-sectional TEM micrograph and the best-fit reflectivity profile after the fitting, respectively. The inset shows the expansion of the NR profile at a low $q_z$. $\chi^2$ calculated from eq 1 was $8.10 \times 10^{-2}$.

**Acknowledgment.** The authors are grateful to NEDO for support through the Japanese National Project "NanoStructured Polymer Project" by the Ministry of Economy, Trade, and Industry and for support from the Ministry of Education, Science, Sports, and Culture through Grants-in-Aid No. 1855019 and No. 19031016. The authors are grateful to Prof. M. Kamigaito and Dr. K. Satoh of Nagoya University for characterizing the volume fraction of the dPS content in the block copolymer. The authors also thank Dr. A. Karim, Dr. R. L. Jones and Dr. B. C. Berry of the U.S. National Institute of Standards and Technology for their valuable comments.

## Appendix

**A. Combination of NR and Cross-Sectional TEM.** In section III, part C, the scattering length density profile evaluated from the TEMT experiment, $b/\upsilon_{\mathrm{TEMT}}$, was used together with the NR profile. It turned out that $b/\upsilon_{\mathrm{TEMT}}$ was an excellent initial "guess". Since the TEMT experiments are tedious and time-consuming, it would be a lot easier if one could use the cross-sectional TEM micrograph alone to evaluate the scattering length density. Therefore, in this Appendix, we tested whether or not the TEM micrograph can be an alternative to the 3D volume data as the initial model in the fitting protocol.

The dashed line in Figure 8a shows the scattering length density profile obtained from the TEM micrograph shown in Figure 4, $b/\upsilon_{\mathrm{TEM}}$. We note here that the TEM micrograph was carefully chosen from the tilt series in the TEMT experiment so that the Si substrate became truly perpendicular to the micrograph. This point is important because the $b/\upsilon_{\mathrm{TEM}}$ would not be accurate if the micrograph were taken with some tilt angle. The dashed line in Figure 8b displays the NR profile based on the $b/\upsilon_{\mathrm{TEM}}$, $R_{\mathrm{TEM}}$. The inset in Figure 8b shows the NR profile in the small $q_z$ region. The $R_{\mathrm{TEM}}$ showed a considerable deviation from the experimentally obtained NR profile, $R_{\mathrm{exp}}$, over the entire range of $q_z$.

Following the same procedure as employed in section III, part C, we used $b/\upsilon_{\mathrm{TEM}}$ as the initial guess. The resulting scattering length density, $b/\upsilon_{\mathrm{TEM-fit}}$, and the corresponding NR profile, $R_{\mathrm{TEM-fit}}$, are shown by the solid lines in Figure 8, parts a and b, respectively. Although a slight improvement was attained in the intermediate and high $q_z$ regions in the $R_{\mathrm{TEM-fit}}$, the agreement was poor, especially for the small $q_z$ (see the inset of Figure 8b). This is in sharp contrast to the results demonstrated in Figure 6 where the $R_{\mathrm{TEMT-fit}}$ showed excellent agreement with the $R_{\mathrm{exp}}$. It was also found that the $b/\upsilon_{\mathrm{TEM-fit}}$ (and $b/\upsilon_{\mathrm{TEM}}$) were different from the $b/\upsilon_{\mathrm{TEMT-fit}}$, indicating that the scattering length density profile was not accurately estimated from the TEM micrograph in the first place. The reason for this inaccurate estimation is obviously the loss of structural information along the *Y*-axis in the TEM micrograph.

## References and Notes

(1) Spontak, R. J.; Patel, N. P. In *Developments in Block Copolymer Science and Technology*; Hamley, I. W., Ed.; John Wiley & Sons Ltd.: Chichester, U.K., and New York, 2004.

(2) Fasolka, M. J.; Mayes, A. M. *Ann. Rev. Mater* **2001**, *31*, 323−355.

(3) Guarini, K. W.; Black, C. T.; Zhang, Y.; Kim, H.; Sikorski, E. M.; Babich, I. V. *J. Vac. Sci. Technol. B* **2002**, *20*, 2788−2792.

(4) Hamley, I. W. *Nanotechnology* **2003**, *14*, R39−R54.

(5) Park, C.; Yoon, J.; Thomas, E. L. *Polymer* **2003**, *44*, 6725−6760.

(6) Stoykovich, M. P.; Muller, M.; Kim, S.; Solak, H. H.; Edwards, E. W.; Pablo, J. J.; Nealey, P. F. *Science* **2005**, *308*, 1442−1446.

(7) Widawski, G.; Rawiso, M.; François, B. *Nature (London)* **1994**, *369*, 387−389.

(8) Freer, E. M.; Krupp, L. E.; Hinsberg, W. D.; Rice, P. M.; Hedrick, J. L.; Cha, J. N.; Miller, R. D.; Kim, H. *Nano Lett.* **2005**, *5*, 2014−2018.

(9) Russell, T. P. *Physica B* **1996**, *221*, 267−283.

(10) Mayes, A. M.; Johnson, R. D.; Russell, T. P.; Smith, S. D.; Satija, S. K.; Majkrzak, C. F. *Macromolecules* **1993**, *26*, 1047−1052.

(11) Russell, T. P.; Anastasiadis, S. H.; Menelle, A.; Felcher, G. P.; Satija, S. K. *Macromolecules* **1991**, *26*, 3929−3936.

(12) Torikai, N.; Noda, I.; Karim, A.; Satija, S. K.; Han, C. C.; Matsushita, Y.; KawaKatsu, T. *Macromolecules* **1997**, *30*, 2907−2914.

(13) Noro, A.; Okuda, M.; Odamaki, F.; Kawaguchi, D.; Torikai, N.; Takano, A.; Matsushita, Y. *Macromolecules* **2006**, *39*, 7654−7661.

(14) Parratt, L. G. *Phys. Rev.* **1954**, *95*, 359−369.

(15) Russell, T. P. *Mater. Sci. Rep.* **1990**, *5*, 171−271.

(16) Karim, A.; Singh, N.; Sikka, M.; Bates, F. S.; Dozier, W. D.; Felcher, G. P. *J. Chem. Phys.* **1994**, *100*, 1620−1629.

(17) Ge, S.; Guo, L.; Rafailovich, M. H.; Sokolov, J.; Peiffer, D. G.; Schwarz, S. A.; Colby, R. H.; Dozier, W. D. *Langmuir* **1999**, *15*, 2911−2915.

(18) Liu, Y.; Zhao, W.; Zheng, X.; King, A.; Singh, A.; Rafailovich, M. H.; Sokolov, J.; Dai, K. H.; Kramer, E. J.; Schwarz, S. A.; Gebizlioglu, O.; Sinha, S. K. *Macromolecules* **1994**, *27*, 4000−4010.

(19) Sivaniah, E.; Hayashi, Y.; Matsubara, S.; Kiyono, S.; Hashimoto, T.; Fukunaga, K.; Kramer, E. J.; Mates, T. *Macromolecules* **2005**, *38*, 1837−1849.

(20) Matsuwaki, U.; Sugimori, H.; Niihara, K.; Nishikawa, Y.; Jinnai, H.; Nishi, T. *Polym. Prepr. Jpn.* **2005**, *54*, 3315−3316.

(21) Knoll, A.; Horvat, A.; Lyakhova, K. S.; Krausch, G.; Sevink, G. J. A.; Zvelindovsky, A. V.; Magerle, R. *Phys. Rev. Lett.* **2002**, *89*, 035501−035504.

(22) Frank, J. In *Principles of Electron Tomography*; Frank, J., Ed.; Plenum Press: New York, 1992.

(23) Jinnai, H.; Ikehara, T.; Nishi, T. *Adv. Polym. Sci.* **2004**, *170*, 115−167.

(24) Kawase, N.; Kato, M.; Nishioka, H.; Jinnai, H. *Ultramicroscopy* **2007**, *107*, 8−15.

(25) Morita, H.; Kawakatsu, T.; Doi, M.; Nishi, T.; Jinnai, H. Submitted for publication.

(26) Spontak, R. J.; Williams, M. C.; Agard, D. A. *Polymer* **1988**, *29*, 387−395.

(27) Radzilowsk, L. H.; Crragher, B. O.; Stupp, S. I. *Macromolecules* **1997**, *30*, 2110−2119.

(28) Kaneko, T.; Suda, K.; Satoh, K.; Kamigaito, M.; Kato, T.; Ono, T.; Nakamura, E.; Nishi, T.; Jinnai, H. *Macromol. Symp.* **2006**, *242*, 80−86.

(29) Yamauchi, K.; Takahashi, K.; Hasegawa, H.; Iatrou, H.; Hadjichristidis, N.; Kaneko, T.; Nishikawa, Y.; Jinnai, H.; Matsui, T.; Nishioka, H.; Shimizu, M.; Furukawa, H. *Macromolecules* **2003**, *36*, 6962−6966.

(30) Jinnai, H.; Sawa, K.; Nishi, T. *Macromolecules* **2006**, *39*, 5815−5819.

(31) Jinnai, H.; Yasuda, K.; Nishi, T. *Macromol. Symp.* **2006**, *245*−*246*, 170−174.

(32) Jinnai, H.; Nishikawa, Y.; Spontak, R. J.; Smith, S. D.; Agard, D. A.; Hashimoto, T. *Phys. Rev. Lett.* **2000**, *84*, 518−521.

(33) Niihara, K.; Nishikawa, Y.; Nishi, T.; Jinnai, H. *Trans. Mater. Res. Soc. Jpn.* **2005**, *30*, 617−622.

(34) Xu, T.; Zvelindovsky, A. V.; Sevink, G. J. A.; Lyakhova, K. S.; Jinnai, H.; Russell, T. P. *Macromolecules* **2005**, *38*, 10788−10798.

(35) Dohi, H.; Kimura, H.; Kotani, M.; Kaneko, T.; Kitaoka, T.; Nishi, T.; Jinnai, H. *Polym. J.* **2007**, *39*, 749−758.

(36) Nishioka, H.; Niihara, K.; Kaneko, T.; Yamanaka, J.; Nishikawa, Y.; Inoue, T.; Nishi, T.; Jinnai, H. *Composite Interfaces* **2006**, *13*, 589−603.

(37) Takeda, M.; Endoh, Y. *Physica B* **1999**, *267*−*268*, 185−189.

(38) Niihara, K.; Kaneko, T.; Suzuki, T.; Sato, Y.; Nishioka, H.; Nishikawa, Y.; Nishi, T.; Jinnai, H. *Macromolecules* **2005**, *38*, 3048−3050.

(39) Kaneko, T.; Nishioka, H.; Nishi, T.; Jinnai, H. *J. Electron Microsc.* **2005**, *54*, 437−444.

(40) Sugimori, H.; Nishi, T.; Jinnai, H. *Macromolecules* **2005**, *38*, 10226−10233.

(41) Luther, P. K.; Lawrence, M. C.; Crowther, R. A. *Ultramicroscopy* **1988**, *24*, 7−18.

(42) Crowther, R. A.; DeRosier, D. J.; Klug, A. *Proc. R. Soc. London* **1970**, *A 317*, 319−340.

(43) Spontak, R. J.; Fung, J. C.; Braunfeld, M. B.; Sedat, J. W.; Agard, D. A.; Kane, L.; Smith, S. D.; Satkowski, M. M.; Ashraf, A.; Hadjuk, D. A.; Gruner, S. M. *Macromolecules* **1996**, *29*, 4494−4507.

(44) Knoll, A.; Tsarkova, L.; Krausch, G. *Nano Lett.* **2007**, *7*, 843−846.

(45) Pasyuk, V. L.; Lauter, H. J.; Gordeev, G. P.; Buschbaum, P. M.; Toperverg, B. P.; Jernenkov, M.; Petry, W. *Langmuir* **2003**, *19*, 7783−7788.

(46) Lee, B.; Park, I.; Yoon, J.; Park, S.; Kim, J.; Kim, K.; Chang, T.; Ree, M. *Macromolecules* **2005**, *38*, 4311−4323.

(47) Wang, J.; Leiston-Belanger, J. M.; Sievert, J. D.; Russell, T. P. *Macromolecules* **2006**, *39*, 8487−8491.

(48) Buschbaum, P. M.; Maurer, E.; Bauer, E.; Cabitt, R. *Langmuir* **2006**, *22*, 9295−9303.

(49) Fukunaga, K.; Elbs, H.; Magerle, R.; Krausch, G. *Macromolecules* **2000**, *33*, 947−953.

(50) Parratt32, http://www.hmi.de.

MA071334C